P H Y S I C A L   R E V I E W   L E T T E R S

Orbital Control of Noncollinear Magnetic Order in Nickel Oxide Heterostructures

A. Frano,[1,2] E. Schierle,[2] M. W. Haverkort,[1] Y. Lu,[1] M. Wu,[1] S. Blanco-Canosa,[1] U. Nwankwo,[1] A. V. Boris,[1] P. Wochner,[1] G. Cristiani,[1] H. U. Habermeier,[1] G. Logvenov,[1] V. Hinkov,[3,†] E. Benckiser,[1] E. Weschke,[2] and B. Keimer[1,*]

[1]*Max-Planck-Institut für Festkörperforschung, Heisenbergstrasse 1, D-70569 Stuttgart, Germany*
[2]*Helmholtz-Zentrum Berlin für Materialien und Energie, Wilhelm-Conrad-Röntgen-Campus BESSY II,*
Albert-Einstein-Strasse 15, D-12489 Berlin, Germany
[3]*Quantum Matter Institute, University of British Columbia, Vancouver, British Colombia V6T 1Z1, Canada*
(Received 3 April 2013; revised manuscript received 10 July 2013; published 5 September 2013)

We have used resonant x-ray diffraction to develop a detailed description of antiferromagnetic ordering in epitaxial superlattices based on two-unit-cell thick layers of the strongly correlated metal $LaNiO_3$. We also report reference experiments on thin films of $PrNiO_3$ and $NdNiO_3$. The resulting data indicate a spiral state whose polarization plane can be controlled by adjusting the Ni d-orbital occupation via two independent mechanisms: epitaxial strain and spatial confinement of the valence electrons. The data are discussed in light of recent theoretical predictions.

The theoretical prediction and experimental control of collective electronic ordering phenomena in metals with strongly correlated electrons are among the greatest challenges of current solid-state physics. Transition metal oxides on the verge of a Mott metal-insulator transition have been of particular interest because of their diverse ground states with different forms of spin, charge, and orbital order. Recent advances in the synthesis of epitaxial metal-oxide heterostructures have provided new opportunities for the controlled exploration of the phase behavior of correlated-electron metals [1,2]. Nickel oxides of composition $RNiO_3$ are a particularly promising platform for these efforts, because they are either metallic and paramagnetic at all temperatures T (R = La), or become Mott-insulating and antiferromagnetic at low T ($R \neq$ La) [3,4]. Recent experimental [5–10] and theoretical [11–20] work has provided initial insights into the phase behavior of $RNiO_3$-based thin films, heterostructures, and superlattices (SLs). In particular, muon spin rotation (μSR) experiments yield evidence of antiferromagnetism in SLs with $LaNiO_3$ (LNO) layers of thickness below three unit cells (u.c.) sandwiched between insulating blocking layers, whereas SLs with thicker LNO layers remain paramagnetic [5]. Exchange-bias effects revealed by magnetometric measurements on heterostructures of LNO and ferromagnetic $LaMnO_3$ also indicate antiferromagnetic or spin-glass order in LNO [6]. These results have stimulated detailed theoretical predictions for the magnetic ordering patterns in nickel oxide heterostructures and SLs. Depending on the chemical composition, dimensionality, and strain state of the $RNiO_3$ layers, various ground states have been predicted, including insulating and metallic antiferromagnets with and without modulation of the magnetic moment amplitude [11–13,19,20]. Since these conditions can be varied in heterostructures to a much greater extent than in bulk solid-state synthesis, a new mode of

research based on close feedback between layer-by-layer synthesis, experimental characterization, and theoretical analysis and prediction appears within reach.

The bottleneck in this new research direction is the experimental characterization of the complex magnetic structures in the atomically thin layers of metal-oxide heterostructures. Most experiments to date have focused on spatially uniform order parameters (such as the uniform magnetization) that modulate the macroscopic properties, and on corresponding layer-to-layer variations which can be determined by neutron or x-ray reflectometry. In contrast, little experimental information is currently available about ordering patterns within the heterostructure layers, including especially those predicted for the nickel oxides [11–13,19,20]. We have used resonant x-ray diffraction (RXD) to develop a detailed, microscopic description of the magnetic ordering patterns in epitaxial superlattices of metallic LNO and thin films of $RNiO_3$ (R = Nd and Pr). In SLs with two adjacent LNO layers, the RXD data reveal a spiral state that is rarely observed in metallic systems and that has thus far not been considered in first-principles calculations (although a closely related state has been reported in bulklike $NdNiO_3$ (NNO) films [21]). We further report initial steps towards control of the antiferromagnetic order by demonstrating that the polarization plane of the spiral can be switched by manipulating the Ni d-orbital occupation via epitaxial strain and spatial confinement. Our RXD data enable detailed tests of theoretical work on the nickel oxides, and provide the foundation for the integration of "orbitally engineered" nickel oxides into spintronic devices.

Superlattices of LNO and insulating, nonmagnetic $LaAlO_3$ (LAO) or $DyScO_3$ (DSO) [22] were grown using pulsed laser deposition on various [001]-oriented substrates: $La(Sr)AlO_4$ (LSAO), $[LaAlO_3]_{0.3}[Sr_2AlTaO_6]_{0.7}$ (LSAT), $SrTiO_3$ (STO), and DSO with in-plane lattice

constants 3.756, 3.87, 3.905, and 3.95 Å, respectively. The substrates and blocking layers allowed us to impose variable levels of compressive or tensile strain on LNO, whose bulk lattice constant is $a = 3.84$ Å. Data on NNO and PrNiO$_3$ (PNO) films with $a = 3.79$ and 3.84 Å, respectively, were taken for comparison. We discuss structural data in terms of the pseudocubic unit cell of the perovskite lattice. The momentum transfer $\mathbf{q} = (H, K, L)$ is also indexed in these units. As demonstrated previously [5,7], the layer sequence of our SLs is defined with u.c. precision. We consider SLs with N u.c. LNO-N u.c. RXO ($N = 2, 3, 4$) structures, labeled ($N \parallel N$) in the following [23].

The RXD experiments were performed at the BESSY-II undulator beam line UE46-PGM1 using variable linearly polarized photons in a horizontal scattering geometry (Fig. 1). A three-circle UHV diffractometer was equipped with a continuous-flow He cryostat. To access the (1/4, 1/4, 1/4) reflection, the [001]-oriented samples were mounted on copper wedges with a 55° tilt. The azimuth value $\psi = 0°$ is assigned when the crystal vectors [1, 1, 1] and $[1, \bar{1}, 0]$ span the scattering plane, and positive rotation around $\mathbf{q}$ is left handed. This geometry precluded full ψ scans, as there are two angular ranges where the incident or outgoing beams are below the sample horizon. In our definition of ψ, these occur around $\psi = 270°$ and 90°, respectively. To estimate the values of the polarization-dependent scattering cross section at these azimuth positions, we used a nontilted (asymmetric) scattering geometry to access part of the (1/4, 1/4, L) scattering rod [23].

Figure 2 shows representative data on the momentum, energy, and temperature dependence of the scattering cross section. Panel (a) displays selected reciprocal-space scans on (2 $\parallel$ 2), (3 $\parallel$ 3), and (4 $\parallel$ 4) SLs taken under resonant
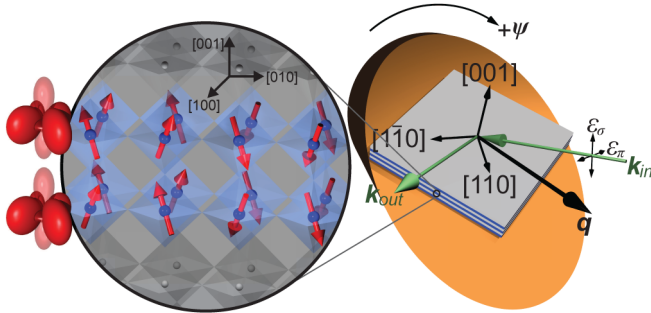

FIG. 1 (color online). Left panel: Schematic diagram of the magnetic structure of a $N = 2$ LNO-RXO SL grown on tensile strain. The Ni moments are illustrated by arrows. Also shown are the electron density distributions in the Ni $d_{x^2-y^2}$ (opaque) and $d_{3z^2-r^2}$ (semitransparent) orbitals. Right panel: Samples were mounted on a tilted wedge to access the [111] direction of the pseudocubic perovskite structure in the horizontal scattering geometry. Also shown are the wave vectors of the incoming and outgoing photons (light arrows), the corresponding momentum transfer $\mathbf{q}$, the incoming photon polarization ε (dark arrows), and the azimuthal angle ψ.

conditions, that is, with the photon energy tuned to the Ni L_3 edge. (2 $\parallel$ 2) SLs of *all* compositions grown on *all* substrates investigated here show resonant Bragg reflections at $\mathbf{q_0} = (1/4, 1/4, L)$, whereas samples with 3 or 4 consecutive u.c. of LNO do not. Comparison of the energy dependence of the diffracted intensity at $\mathbf{q_0}$ with x-ray absorption spectroscopy (XAS) data [Fig. 2(b)] confirms the resonance at the Ni L_3 edge, and the polarization dependence of the scattering cross section (see below) confirms the magnetic origin of the Bragg reflections. The observation of magnetic Bragg reflections implies staggered ordering of the Ni moments in the SL plane analogous to the one characterizing antiferromagnetic order in bulk nickel oxide perovskites [4,21] and rules out a spin glass state that has been considered in related SLs [6]. The observation of a scattering rod perpendicular to the SL plane [inset in Fig. 2(a)] is consistent with quasi-two-dimensional spin correlations, but the accessible range of the corresponding momentum transfer, L, is not sufficient to determine the spin-spin correlation length in this direction. The temperature dependence of the integrated peak intensity [Fig. 2(c)] shows a pronounced tail above the Néel temperature of ~50 K determined by μSR on the same sample [5,23]. Measurements of the peak width [23] indicate that this originates from dynamical short-range order with strongly T-dependent in-plane correlation length, which is typical for quasi-two-dimensional magnets [24].

In order to determine the magnetic moment direction, we systematically varied the incoming and outgoing photon polarization vectors, ε and ε', relative to the electronic magnetic moments by scanning the azimuthal angle ψ around $\mathbf{q_0}$ (Fig. 1). The intensity of a magnetic Bragg reflection is given by [25]

$$I_{kl} = | \sum_j e^{i\mathbf{q} \cdot \mathbf{r}_j} \varepsilon'_l \cdot F_j(E) \cdot \varepsilon_k |^2, \tag{1}$$

with $k, l \in \{\sigma, \pi\}$. Figure 2(b) shows that the energy profiles of the Bragg reflections measured at different azimuthal angles ψ are identical. This confirms that the Bragg intensity at $\mathbf{q_0}$ arises from a single set of scattering tensors $F_j(E)$ at lattice site j, which (together with the corresponding phase factors) encode the magnetic ordering pattern. We measured the scattered intensity for σ- and π-polarized incident photons (Fig. 1), so that the two channels $\boldsymbol{\pi} \equiv I_{\pi\sigma} + I_{\pi\pi}$ and $\boldsymbol{\sigma} \equiv I_{\sigma\pi}$ were distinguished. We present the measured data as the ratio $\boldsymbol{\pi}/\boldsymbol{\sigma}$, which is not influenced by the shape of the sample and the orientation of its surfaces relative to the incoming and outgoing x-ray beams, and can thus be directly compared to model calculations.

Figure 3 displays the polarization-dependent data for different LNO-based SLs with $N = 2$ and films exhibiting antiferromagnetic order, grown on substrates that impose either tensile [Fig. 3(a)] or compressive [Figs. 3(b) and 3(c)] strain. The blue line in Fig. 3(c) represents the result of a calculation for the magnetic structure of bulk RNiO$_3$ with
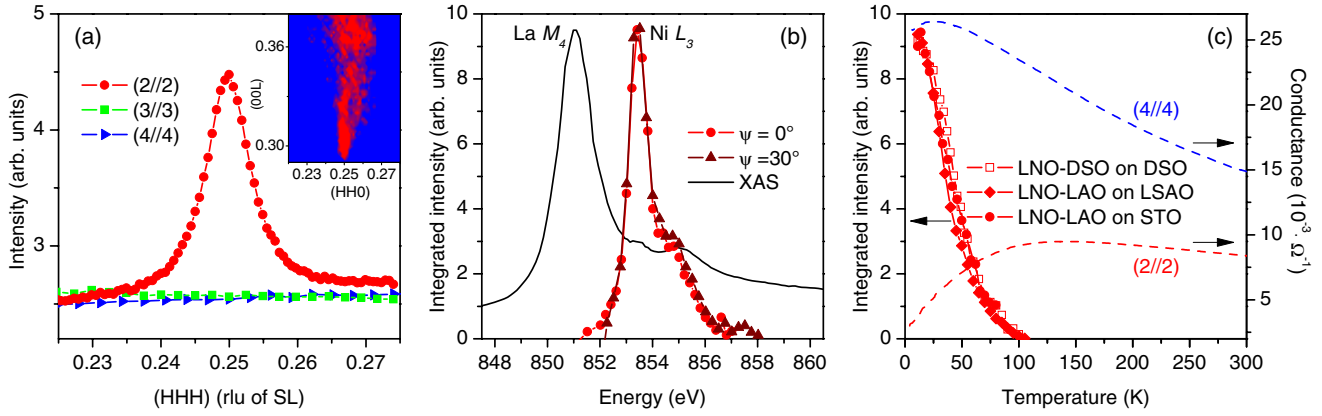
FIG. 2 (color online).   (a) Scans around $\mathbf{q_0} = (1/4, 1/4, L)$ at $T = 10$ K and $E = 853.4$ eV for SLs with composition LNO-LAO, LNO-DSO, and $N = 2$ consecutive LNO unit cells show a magnetic Bragg reflection, while those with $N = 3, 4$ do not. The inset shows a reciprocal-space map of the scattered intensity from the $N = 2$ SL. (b) Comparison between the x-ray absorption spectroscopy (XAS) and the photon-energy dependence of the magnetic Bragg intensity at $\mathbf{q_0}$ close to the Ni L_3 ($2p \rightarrow 3d$) edge, which shows almost identical line shapes for two azimuthal angles $\psi = 0, 30°$. (c) Temperature dependence of the magnetic Bragg intensity at $\mathbf{q_0}$ in LNO-based SLs with $N = 2$ (symbols), compared to representative dc electrical conductance measurements (taken by a standard four-probe method) for $N = 2$ and $N = 4$ SLs (dashed lines).

$R \neq$ La [4,21], which comprises two sets of spirals polarized perpendicular to the propagation vector $\mathbf{q_0}$ [blue arrows in Fig. 3(f)]. Whereas the magnetic structure of 2 u.c.-LNO confined between LAO layers under compressive strain is compatible with the one in the bulk [Fig. 3(c)], the data sets on all samples grown under tensile-strain conditions [Fig. 3(a)], and the one of a pure NNO film grown under compressive strain [Fig. 3(b)], indicate distinctly different magnetic structures.

In analyzing the azimuthal scans of Fig. 3, we considered both collinear antiferromagnetic structures with spatial variation of the moment amplitude and spiral structures analogous to the one in bulk RNiO$_3$ with identical amplitude on every lattice site [see Figs. 3(a) and 3(b)]. Model calculations [11,12] show that the relative stability of these two structures depends on factors that are difficult to compute from first principles, such as the on-site correlation strength. The comprehensive data sets displayed in Fig. 3 allow an experimental test of these predictions. Whereas collinear structures turned out to be incompatible with the data [see dashed lines in Figs. 3(a) and 3(b)], calculations based on spiral states yield excellent descriptions of all three distinct data sets [solid lines in Figs. 3(a) and 3(b)]. These structures can be derived from the structure of bulk RNiO$_3$ by adjusting the direction of the moments in the two sublattices. In the best fits for all samples under tensile strain, the moments are symmetrically tilted from the [001] axis by $28 \pm 2°$ [red arrows in Fig. 3(d)], and remain coplanar with those of the bulk structure [26]. The magnetic structure of the NNO sample under compressive strain, on the other hand, comprises moments along [110] and [1$\bar{1}$0] [green arrows in Fig. 3(e)]. Note the striking difference between the polarization plane of this sample and the one of the LNO-LAO SL shown in Fig. 3(f), which was grown on

the same substrate (LSAO) and exhibits the same in-plane lattice parameter.

In order to uncover the origin of the surprising variability of the helical polarization plane, we used x-ray absorption spectroscopy with linearly polarized x rays near the Ni L_2 edge to determine the relative occupation of the Ni d-orbitals, which controls the magnetocrystalline anisotropy via the spin-orbit coupling [27,28]. Figures 3(g)–3(i) display the difference of the absorption spectra for photons polarized parallel and perpendicular to the substrate surface for three representative samples, normalized by the averaged energy integral. Taking advantage of the sum rule for linear dichroism, we have converted the energy integrals into the ratio of e_g hole occupation numbers $X \equiv \underline{n}_{3z^2-r^2}/\underline{n}_{x^2-y^2}$ [29]. The SLs and films grown under tensile strain show $1.03 \leq X \leq 1.14$, corresponding to an enhanced electron occupation of the $d_{x^2-y^2}$ orbital [Fig. 3(g)]. Since orbital moments in this situation will point along z, the experimentally observed canting of the spin moments towards this direction [Fig. 3(d)] is a natural consequence of the intra-atomic spin-orbit coupling. Conversely, the preferential $d_{3z^2-r^2}$ occupation ($X = 0.97$) found in the compressively strained NNO film [Fig. 3(h)] accounts for the observed spin polarization in the x, y plane [Fig. 3(e)]. In the compressively strained LNO-LAO SL, our data show that the equal population of $d_{x^2-y^2}$ and $d_{3z^2-r^2}$ found in bulk nickel oxides is restored [Fig. 3(i)], consistent with prior reports on related SLs [9] and with the bulklike magnetic structure of this sample [Fig. 3(f)]. This requires a mechanism that counteracts the effect of compressive strain observed in the NNO film on the same substrate. Such a mechanism has been identified in model calculations for LNO-based SLs, [14,15,17] which indicate that the confinement of the LNO conduction electrons to the x, y plane by the insulating
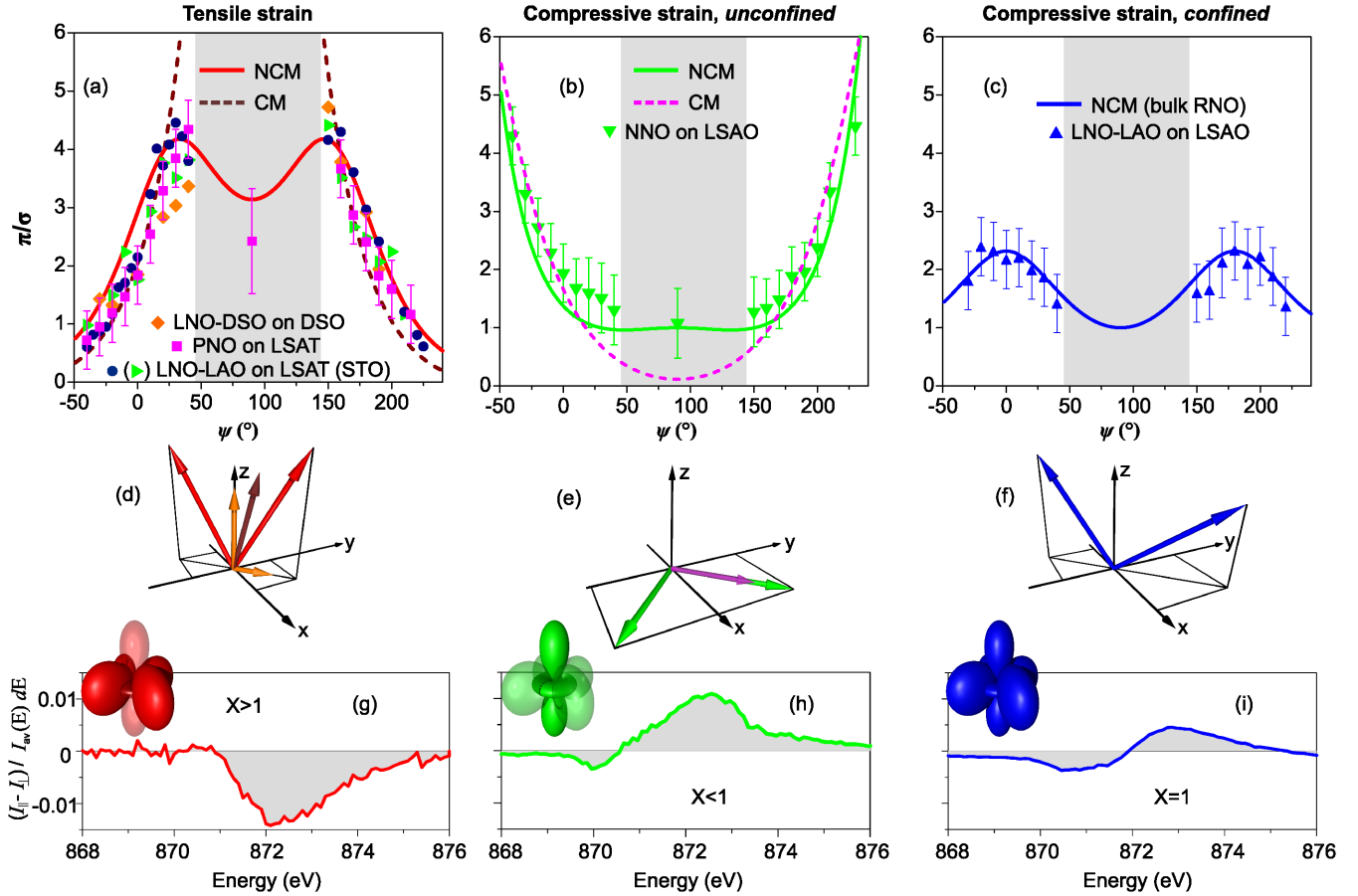
FIG. 3 (color online).   (a)–(c) Dependence of the polarization dependent scattering intensity π/σ on the azimuthal angle ψ for LNO-based SLs and a PNO film on LSAT (tensile strain), (b) a NNO film on LSAO (compressive strain, unconfined), and (c), a LNO-LAO SL on LSAO (compressive strain, confined). The solid (dashed) lines represent the results of fits to noncollinear (collinear) magnetic structure models described in the text. In the shaded areas around $\psi = 90°$, measurements were not possible in the tilted scattering geometry of Fig. 1, and an alternative geometry was used (see text). (d)–(f) Sketches of the spin directions in the two-sublattice magnetic structure resulting from the fits. The color-coding refers to panels (a)–(c) [26]. (g)–(i) Linear dichroism obtained from XAS measurements around the Ni L_2 edge with incoming light polarization in and out of the substrate plane, normalized by the polarization-averaged energy integral. The ratio X of orbital occupations derived from the sum rule (see text) is given in the legend and schematically depicted by color-coded solid and semitransparent plots of the corresponding electron density distribution.

blocking layers of the SL stabilizes the $d_{x^2-y^2}$ orbital relative to $d_{3z^2-r^2}$. In contrast to the long-range effect of epitaxial strain, recent results from resonant x-ray reflectometry [7,30] indicate that the orbital polarization is spatially modulated due to the dimensional confinement which predominantly acts on the interface layers, thus affording an independent means of controlling the spin polarization.

In summary, our RXD data have allowed us to develop a detailed picture of the complex in-plane magnetic super-structures in atomically thin nickel-oxide layers. The quasi-two-dimensional, noncollinear antiferromagnetic structure we have observed emerges upon cooling out of a metallic high-temperature state (Fig. 2(c) and Ref. [5]) and is therefore consistent with theoretical predictions for spin density wave (SDW) formation. The magnetic propagation vector matches the Fermi surface nesting vector [11–13,16], further supporting this interpretation.

The disappearance of the SDW order in $N = 3$ and $N = 4$ SLs can then be attributed to less favorable nesting conditions of the increasingly three-dimensional Fermi surfaces. The substantial electrical conductivity at low T (Fig. 2(c) and Ref. [5]) may indicate a SDW state with a partially gapped Fermi surface, which has been predicted by *ab initio* calculations [12,20]. Further research is required to assess whether the conductivity maximum at higher temperatures is associated with charge order [31], or with the onset of two-dimensional short-range order [23].

Whereas the *ab initio* calculations have thus far focused on amplitude-modulated states, analytical strong-coupling calculations have shown that spiral order can emerge as a consequence of competing nearest- and next-nearest-neighbor exchange interactions [11]. Spiral order is rare in metallic oxides, but has also been observed in the stoichiometric perovskites $CaFeO_3$ [32], $SrFeO_3$ [33],

and $Sr_3Fe_2O_7$ [34], which bridge a bandwidth-driven Mott transition. Note that the latter compound exhibits a bilayer structure akin to the one of our $N = 2$ SLs. This suggests a common magnetic phenomenology of clean, correlated metals near the onset of localization, which should be further explored experimentally and theoretically.

We have also demonstrated first steps towards control of the noncollinear spin polarization by virtue of two independent mechanisms, epitaxial strain and spatial confinement. Since the nickel oxides can be epitaxially integrated with other metallic oxides exhibiting ferromagnetic or superconducting order, the control options we have identified provide new perspectives for spintronic devices. In view of the substantial conductivity in the SDW state, these may eventually include devices with electronically active antiferromagnetic elements [35].

*b.keimer@fkf.mpg.de
†Present address: Physikalisches Institut und Röntgen Center for Complex Materials Systems, Universität Würzburg, 97074 Würzburg, Germany.

[1] J. Mannhart and D. G. Schlom, Science **327**, 1607 (2010).
[2] H. Y. Hwang, Y. Iwasa, M. Kawasaki, B. Keimer, N. Nagaosa, and Y. Tokura, Nat. Mater. **11**, 103 (2012).
[3] J. B. Torrance, P. Lacorre, A. I. Nazzal, E. J. Ansaldo, and C. Niedermayer, Phys. Rev. B **45**, 8209 (1992).
[4] J. L. García-Muñoz, J. Rodríguez-Carvajal, and P. Lacorre, Europhys. Lett. **20**, 241 (1992).
[5] A. V. Boris, Y. Matiks, E. Benckiser, A. Frano, P. Popovich, V. Hinkov, P. Wochner, M. Castro-Colin, E. Detemple, V. K. Malik, C. Bernhard, T. Prokscha, A. Suter, Z. Salman, E. Morenzoni, G. Cristiani, H.-U. Habermeier, and B. Keimer, Science **332**, 937 (2011).
[6] M. Gibert, P. Zubko, R. Scherwitzl, J. Íñiguez, and J.-M. Triscone, Nat. Mater. **11**, 195 (2012).
[7] E. Benckiser, M. W. Haverkort, S. Brueck, E. Goering, S. Macke, A. Frano, X. Yang, O. K. Andersen, G. Cristiani, H.-U. Habermeier, A. V. Boris, I. Zegkinoglou, P. Wochner, H.-J. Kim, V. Hinkov, and B. Keimer, Nat. Mater. **10**, 189 (2011).
[8] R. Scherwitzl, S. Gariglio, M. Gabay, P. Zubko, M. Gibert, and J.-M. Triscone, Phys. Rev. Lett. **106**, 246403 (2011).
[9] J. W. Freeland, J. Liu, M. Kareev, B. Gray, J. W. Kim, P. Ryan, R. Pentcheva, and J. Chakhalian, Europhys. Lett. **96**, 57004 (2011).
[10] J. Chakhalian, J. M. Rondinelli, J. Liu, B. A. Gray, M. Kareev, E. J. Moon, N. Prasai, J. L. Cohn, M. Varela, I. C. Tung, M. J. Bedzyk, S. G. Altendorf, F. Strigari, B. Dabrowski, L. H. Tjeng, P. J. Ryan, and J. W. Freeland, Phys. Rev. Lett. **107**, 116805 (2011).
[11] S. B. Lee, R. Chen, and L. Balents, Phys. Rev. Lett. **106**, 016405 (2011).
[12] S. B. Lee, R. Chen, and L. Balents, Phys. Rev. B **84**, 165119 (2011).
[13] D. Puggioni, A. Filippetti, and V. Fiorentini, Phys. Rev. B **86**, 195132 (2012).
[14] J. Chaloupka and G. Khaliullin, Phys. Rev. Lett. **100**, 016404 (2008).
[15] P. Hansmann, X. Yang, A. Toschi, G. Khaliullin, O. K. Andersen, and K. Held, Phys. Rev. Lett. **103**, 016401 (2009).
[16] P. Hansmann, A. Toschi, X. Yang, O. K. Andersen, and K. Held, Phys. Rev. B **82**, 235123 (2010).
[17] M. J. Han, C. A. Marianetti, and A. J. Millis, Phys. Rev. B **82**, 134408 (2010).
[18] M. J. Han, X. Wang, C. A. Marianetti, and A. J. Millis, Phys. Rev. Lett. **107**, 206804 (2011).
[19] S. Dong and E. Dagotto, Phys. Rev. B **87**, 195116 (2013).
[20] B. Lau and A. J. Millis, Phys. Rev. Lett. **110**, 126404 (2013).
[21] V. Scagnoli, U. Staub, A. M. Mulders, M. Janousch, G. I. Meijer, G. Hammerl, J. M. Tonnerre, and N. Stojic, Phys. Rev. B **73**, 100409(R) (2006).
[22] In $DyScO_3$ magnetic order was observed below 3.1 K, i.e., outside the temperature range investigated here [X. Ke, C. Adamo, D. G. Schlom, M. Bernhagen, R. Uecker, and P. Schiffer, Appl. Phys. Lett. **94**, 152503 (2009)].
[23] See Supplemental Material at http://link.aps.org/supplemental/10.1103/PhysRevLett.111.106804 for further details.
[24] R. J. Birgeneau, H. J. Guggenheim, and G. Shirane, Phys. Rev. B **1**, 2211 (1970).
[25] M. W. Haverkort, N. Hollmann, I. P. Krug, and A. Tanaka, Phys. Rev. B **82**, 094403 (2010).
[26] For tensile strain, our simulation yields an identical solution for a structure with spin sublattices lying along [001] and [110] and magnetic moment amplitudes that differ by a factor ~ 2 [small, light arrows in Fig. 3(d)]. Additional work is required to elucidate whether the charge disproportionation between neighboring sites implied by the different moment amplitudes is present in our SLs.
[27] P. Bruno, Phys. Rev. B **39**, 865 (1989).
[28] S. I. Csiszar, M. W. Haverkort, Z. Hu, A. Tanaka, H. H. Hsieh, H.-J. Lin, C. T. Chen, T. Hibma, and L. H. Tjeng, Phys. Rev. Lett. **95**, 187205 (2005).
[29] G. van der Laan, J. Phys. Soc. Jpn. **63**, 2393 (1994).
[30] M. Wu, E. Benckiser, M. W. Haverkort, A. Frano, Y. Lu, U. Nwankwo, S. Brück, P. Audehm, E. Goering, S. Macke, V. Hinkov, P. Wochner, G. Christiani, S. Heinze, G. Logvenov, H.-U. Habermeier, and B. Keimer, arXiv:1308.6389.
[31] V. Scagnoli, U. Staub, M. Janousch, A. M. Mulders, M. Shi, G. I. Meijer, S. Rosenkranz, S. B. Wilkins, L. Paolasini, J. Karpinski, S. M. Kazakov, and S. W. Lovesey, Phys. Rev. B **72**, 155111 (2005).
[32] P. M. Woodward, D. E. Cox, E. Moshopoulou, A. W. Sleight, and S. Morimoto, Phys. Rev. B **62**, 844 (2000).
[33] M. Reehuis, C. Ulrich, A. Maljuk, C. Niedermayer, B. Ouladdiaf, A. Hoser, T. Hofmann, and B. Keimer, Phys. Rev. B **85**, 184109 (2012); A. Lebon, P. Adler, C. Bernhard, A. V. Boris, A. V. Pimenov, A. Maljuk, C. T. Lin, C. Ulrich, and B. Keimer, Phys. Rev. Lett. **92**, 037202 (2004).
[34] D. C. Peets, J.-H. Kim, P. Dosanjh, M. Reehuis, A. Maljuk, N. Aliouane, C. Ulrich, and B. Keimer, Phys. Rev. B **87**, 214410 (2013).
[35] A. H. MacDonald and M. Tsoi, Phil. Trans. R. Soc. A **369**, 3098 (2011).